



**Environmental
Science**
Water Research & Technology

**Emerging investigator series: Local pH Effects on Carbon
Oxidation in Capacitive Deionization Architectures**

Journal:	<i>Environmental Science: Water Research & Technology</i>
Manuscript ID	EW-ART-01-2021-000005.R1
Article Type:	Paper

SCHOLARONE™
Manuscripts

Water Impact Statement

The development of more efficient water treatment processes is needed for many desalination and separation applications. Capacitive deionization (CDI) and membrane-assisted capacitive deionization (MCDI) may offer advantages over current processes with proper electrode and system design. In this work, the influence of ion exchange membranes on the local pH and carbon electrode stability is elucidated in CDI and MCDI cells.

Emerging investigator series: Local pH Effects on Carbon Oxidation in Capacitive Deionization Architectures

Authors: James Landon^{a, b, *}, Xin Gao^a, Ayokunle Omosebi^a, Kunlei Liu^{a, c, *}

a: University of Kentucky Center for Applied Energy Research, 2540 Research Park Drive, Lexington, KY 40511, USA

b: Department of Chemical and Materials Engineering, University of Kentucky, 151 Ralph G. Anderson Building, Lexington, KY 40506, USA

c: Department of Mechanical Engineering, University of Kentucky, 151 Ralph G. Anderson Building, Lexington, KY 40506, USA

*james.landon@uky.edu

*kunlei.liu@uky.edu

Keywords: capacitive deionization, carbon oxidation, oxygen reduction, pH response, ion exchange membranes

Abstract

In this work, the effect of pH and potential is examined for the oxidation of carbon cloth electrodes used in capacitive deionization (CDI) processes. The degree of oxidation of the electrode surface, examined using the electrode's potential of zero charge (E_{pzc}) and measured using chronoamperometry and cyclic voltammetry, is found to be strongly correlated to the pH

of the solution at the interface. Local pH measurements are examined at anodes and cathodes in full CDI and membrane-assisted capacitive deionization (MCDI) cells at cell voltages ranging from 0.3-1.2 V. The cathode is shown to be basic under charging potentials while the anode is found to be acidic. This local pH is found to be highly transient during charging and discharging in CDI cells while the pH is found to be relatively static in the MCDI cells, maintaining a basic pH at the cathode and an acidic pH at the anode even when the cell is discharged. Ion exchange membranes (IEM) are found to have two functions: (1) limiting co-ion expulsion that results from specific ion adsorption and (2) limiting the effects of parasitic Faradaic reactions on the separation process by stabilizing the local pH thereby mitigating dissolved oxygen reduction at the cathode and lessening carbon oxidation at the anode. Performance comparisons including the salt adsorption capacity and charge efficiency are also compared for these systems.

Introduction

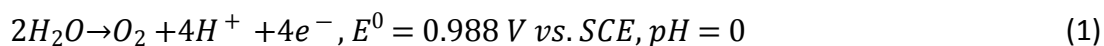
Access to clean water continues to be an ever-increasing global issue. New and innovative solutions to water treatment are needed to address biological, suspended solids, organics, hard mineral, and bulk salt removal in a variety of applications such as brackish water treatment, seawater desalination, irrigation, and specific ion removal, among others. While conventional methods such as multi-stage flash distillation remain in use even as membranes become more common for bulk water treatment, new methods will need to be used to address the shortcomings of all existing methods.

Nanofiltration and reverse osmosis (RO) hold many advantages over previous and emerging water treatment methods, including operating within twofold of the thermodynamic minimum energy required for separation.¹ RO has become the separation method of choice for seawater desalination, largely in part due to the low energy requirements. However, pretreatment required for these membranes can be quite extensive, specifically necessitating chlorine removal for municipal water treatment processes and addressing hard mineral content that can result in scaling of the membrane surface. Capacitive deionization (CDI) and membrane-assisted capacitive deionization (MCDI) may offer some unique advantages over membrane-based technologies due to the removal mechanism where cations and anions are adsorbed to opposing interfaces, decreasing the likelihood of interactions at a sole interface.²⁻⁴ Research in CDI and MCDI systems has classically been carried out on carbon electrodes, cell designs, operation and simulation, and new materials developments.⁵⁻¹⁵ Recent works have focused on the importance of energy efficiency in the assessment of new water treatment methods.¹⁶⁻²² Moreover, selective ion removal may be accomplished more easily through some of the mechanisms available at these more discrete interfaces.^{1, 23, 24}

Gaining insights into the pH swings caused by electrochemical reactions in a CDI cell is critically important in order to achieve efficient, reliable, and stable salt separation processes.²⁵⁻²⁹ Carbon oxidation at the anode and dissolved oxygen reduction at the cathode in a CDI cell are two of the classically studied reactions that trigger pH swings, adversely impacting the energy efficiency, adsorption efficiency, and operating stability.³⁰⁻³³ For instance, as demonstrated in **Figure 1(a)**, dissolved oxygen reduction at the cathode increases the solution's pH with the production of OH⁻, possibly exacerbating carbon oxidation at the anode in certain CDI configurations, e.g., flow-

through, due to a decrease in the Nernstian potential for carbon oxidation when OH^- migrates toward the anode.³⁴ In contrast, these co-ions are repelled in the MCDI configuration (**Figure 1(b)**). While dissolved oxygen is shown to permeate the cation exchange membrane at the cathode, this permeation is largely mitigated using commercially available ion exchange membranes, as shown in previous works.^{4, 27} Therefore, dissolved oxygen reduction is expected to be low at the cathode in MCDI. As is now generally accepted, degradation in CDI performance is mainly accounted for by anodic carbon oxidation, so mitigating this reaction from occurring has become paramount.^{30, 31} Therefore, if possible, carbon electrode and cell designs should be adapted that control the effect of parasitic reaction products and take into account the nearly inevitable pH swings that occur at each electrode interface.

The pH of a solution has a direct impact on the Nernst potential for many electrochemical reactions. In addition, cell potentials in CDI and MCDI systems are generally kept below 1.229 V to theoretically avoid oxygen evolution at the anode (positive electrode) and hydrogen evolution at the cathode (negative electrode). Oxygen evolution reaction potentials are shown in Eq. (1) and (2) for solution pH of 0 and 14, respectively.

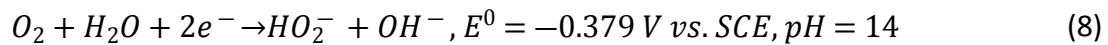
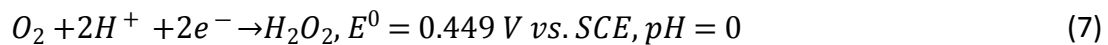
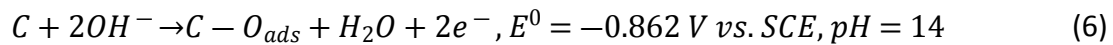
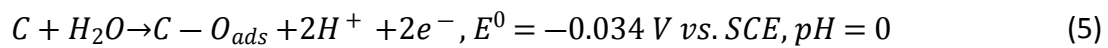


Reactions can also be written for hydrogen evolution as a function of solution pH, which are shown in Eq. (3) and (4) for solution pH of 0 and 14, respectively.





Due to the overpotentials for these two and four-electron reactions as well as the cell potentials used to conduct the separation process, gaseous products are generally not expected in CDI and MCDI cells. However, other two-electron processes such as carbon oxidation at the anode and oxygen reduction at the cathode have been shown to occur. These pH-dependent reactions are shown in Eq. (5-6) for the carbon oxidation and Eq. (7-8) for the oxygen reduction.²⁸



Therefore, while gaseous products are unlikely to form, there exist multiple Faradaic reactions that can and do occur in CDI systems.²⁷⁻²⁹ Monitoring and mitigation of these reactions and the subsequent deleterious separation effects they cause is necessary to ensure a long-lasting and efficient separation process.

Through this work, pH-dependent reactions at carbon anodes and cathodes are probed in both flow-by CDI and MCDI cells. Local pH measurements are used to explain and quantify parasitic reactions at each electrode that induce efficiency losses for the separation process, building upon previous work that focused solely on the CDI architectures.³⁵ MCDI cells are shown to have not only higher charge efficiencies due to the mitigation of co-ion expulsion but also the ability of ion exchange membranes (IEM) to limit the pH swing resulting from parasitic reactions at the

electrode interfaces and retaining preferential reaction products at the electrode interface. IEMs are further shown to maintain a near-constant pH at the electrode interface under charging/discharge conditions in MCDI, which is in direct contrast to the transient pH responses seen in a conventional flow-by CDI configuration. The magnitude of transient local pH measurements is measured in both CDI and MCDI configurations as a function of cell potential for the first time. Suggestions on how to improve separation and energy efficiencies are proposed.

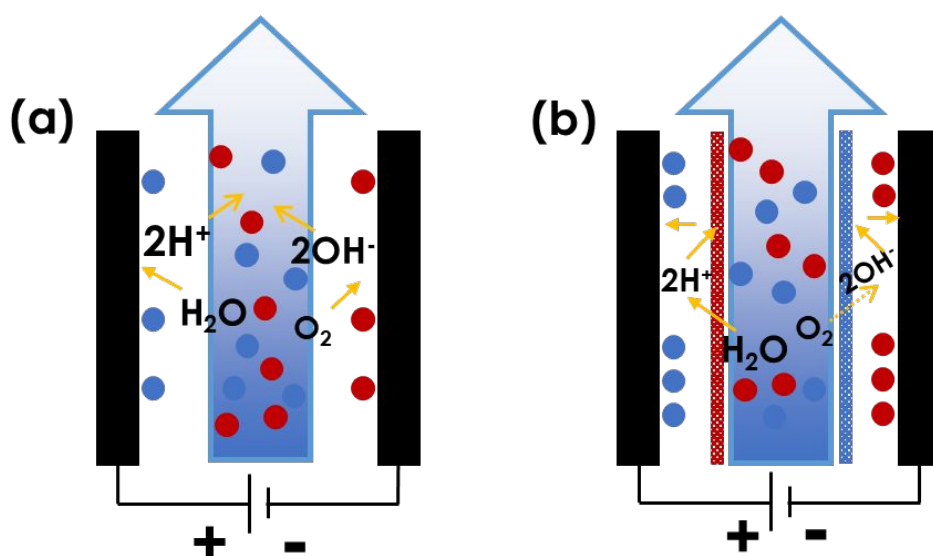


Figure 1. pH influence for (a) CDI vs (b) MCDI cells. H^+ generated at the anode and OH^- generated at the cathode have direct access to the bulk solution in CDI cells while these species are hindered in MCDI cells due to the presence of ion exchange membranes.

Materials and Methods

Electrochemical Characterization

Electrochemical tests were performed using a three-electrode cell configured with Kynol carbon cloth electrodes with the areal size of $0.6 \times 0.6 \text{ cm}^2$ (or mass of approximately 0.005 g), a saturated calomel electrode (SCE), and a titanium mesh counter electrode. All three electrodes were connected to an Autolab PGSTAT128N potentiostat.

To investigate the effect of solution pH on carbon oxidation, chronoamperometry was carried out at 0.8 V vs. SCE for 32,000 s in 40 mL of NaCl solution with the pH adjusted to 10.1 and 3.3 using either NaOH or HCl with a total ionic strength of 4.3 mM. These pH values were chosen to reflect the more extreme local pH conditions seen at the carbon cloth electrode interfaces. Subsequently, after chronoamperometry at this oxidizing potential, the carbon cloth electrode was rinsed with a copious amount of deionized water followed by conducting cyclic voltammetry at 0.5 mV s^{-1} from -1.0 V to 1.0 V vs. SCE in 40 mL of 4.3 mM NaCl solution. To evaluate the used (or cycled) electrodes from both the MCDI and CDI cells, the used electrode was resized into $0.6 \times 0.6 \text{ cm}^2$ to assemble a similar three-electrode cell as mentioned above. Cyclic voltammetry was then conducted at 0.5 mV s^{-1} from -0.6 V to 0.8 V vs. SCE in 40 mL of 4.3 mM NaCl solution.

Construction of pH Cell

A specially designed pH cell was used to investigate local pH conditions at the anode and cathode in both CDI and MCDI cells. Shown below in **Figure 2** is a general schematic of the cell used in this study with actual pictures of the cell shown in **Figure S4**. Orion AquaPro™ flat-surface pH probes were purchased from Thermo Scientific to measure the local pH conditions at the anode and cathode. The cell stack consisted of grade 2 titanium mesh, Kynol carbon cloth electrode, a

porous nylon mesh purchased from McMaster Carr with a thickness of approximately 100 μm , a second Kynol carbon cloth electrode, and a second grade 2 titanium mesh. The flat-surface pH probes accessed the local pH conditions at the anode and cathode through a $\sim 1\text{ cm}^2$ circular hole cut in the titanium mesh with the probe tips situated directly at the back of the carbon electrodes. By measuring the conditions at the back of the carbon cloth electrode, local pH conditions could be better resolved instead of being in the direct solution flow path. Transient pH responses showed that pH measurements were relevant to the solution-accessible electrode surface. Salt solution was fed through the bottom of the cell in a flow-by configuration and exited through the top of the cell. The only change from the CDI cell to the MCDI cell was the inclusion of a Neosepta AMX anion exchange membrane covering the anode and a Neosepta CMX cation exchange membrane covering the cathode to sandwich the porous separator. The carbon cloth dimensions were 5 cm x 5 cm with the ion exchange membranes being similar but slightly larger in dimension.

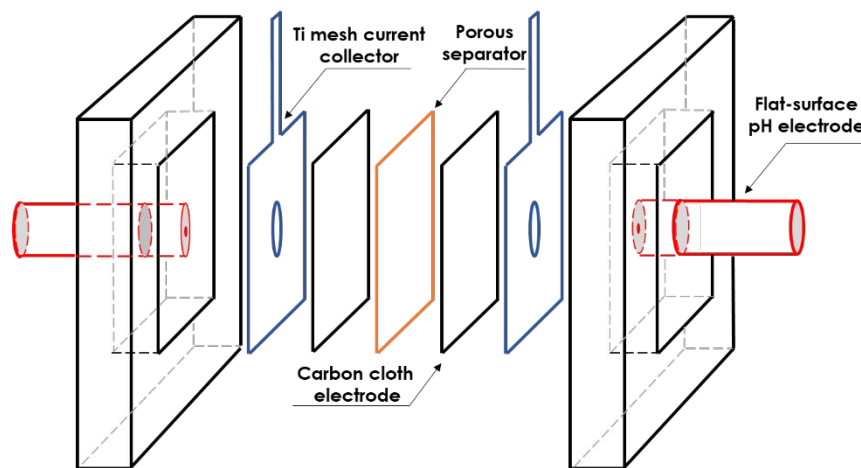


Figure 2. The cell is symmetrically separated by a porous separator. Each half-cell consists of a carbon cloth electrode, a Ti mesh current collector, and a flat-surface pH electrode.

Capacitive Deionization Characterization

CDI and MCDI studies were carried out using the cell described above with the sole difference being the inclusions of Neosepta AMX and CMX ion exchange membranes being used in the MCDI cell. The solution used for adsorption/desorption studies was 400 ml of 4.3 mM NaCl. Solution was recirculated at a flow rate of approximately 20 ml/min through the system in a batch-mode type flow path. The total carbon mass used in the experiment was about 0.6 g in both the CDI and MCDI studies, with new carbon being used for each experiment. Charging and discharging was carried out at 30 min for each step. Charging potentials of 0.3, 0.6, 0.9, and 1.2 V were used while discharge was carried out solely at short-circuit, 0 V. A minimum of three cycles at each charging potential was conducted. Current, conductivity, and the local pH at the anode and cathode were logged at a rate of 0.2 Hz. The salt adsorption capacity (SAC, mg NaCl/g electrode) and charge efficiency (Λ) were calculated using equations 9 and 10, respectively.

$$SAC = \frac{A \times MW_{NaCl} \times \Delta\sigma \times V}{m} \quad (9)$$

$$\Lambda = \frac{SAC \times F / MW_{NaCl}}{Q} \times 100 \quad (10)$$

where A is a calibration parameter (8.87×10^{-3} mol·cm·mg/L· μ S·g), MW_{NaCl} is the molecular weight of sodium chloride in g/mol, $\Delta\sigma$ is the change in conductivity during the charging cycle in μ S/cm, V is the solution volume in L, m is the mass of carbon electrode in g, F is Faraday's constant (96,485 C/mol), and Q is the charge passed per gram of carbon in C/g. The SAC is calculated to be mg of salt per gram of carbon. The value is converted to be gram of salt per gram of carbon in the calculation of the charge efficiency. A calibration plot of NaCl concentration vs. conductivity is shown in **Figure S5**.

Results and Discussion

To examine the effect of pH on carbon oxidation, stepped potential studies were conducted using a three-electrode cell and chronoamperometry in electrolytes with varying pH. The potential of zero charge (E_{pzc}) of the carbon electrode was examined through cyclic voltammetry both before and after the stepped potential. A positive shift in the E_{pzc} signals oxidation of the electrode surface, something that has been shown in multiple previous works.^{30, 31} Shown in **Figure 3a** is the current density of a microporous carbon cloth working electrode with 0.8 V vs. SCE being applied in both pH 10.1 and 3.3 NaCl electrolytes with the total ionic strength being held constant at 4.3 mM. This step potential was held for 32,000 s, approximately 8.9 hours, in each electrolyte. The steady-state current density, resulting mainly from Faradaic reactions, is found to be 18.6 mA/g and 16.4 mA/g for the pH 10.1 and pH 3.3 electrolytes, respectively, after 30,000 s. Such an observation indicates that, at a pH of 10.1, the pH-dependent carbon oxidation reaction written in Eq. (6) would have a Nernstian potential of -0.632 V vs. SCE, providing an overpotential of 1.432 V. Likewise, at a pH of 3.3, the Nernstian potential would be -0.228 V vs. SCE, reducing the overpotential to 1.03 V. The noted current density is approximately 13% higher at a pH of 10.1, resulting from the higher overpotential of reaction seen in this electrolyte. As shown in **Figure 3b**, the E_{pzc} , typically found -0.1-0.1 V vs. SCE for the pristine carbon cloth electrode,^{12, 29} is shown to have shifted to nearly 0.3 V vs. SCE for the pH 3.3 solution and close to 0.4 V vs. SCE for the pH 10.1 solution, demonstrating the impact of overpotential on the resulting oxidation of the carbon surface.

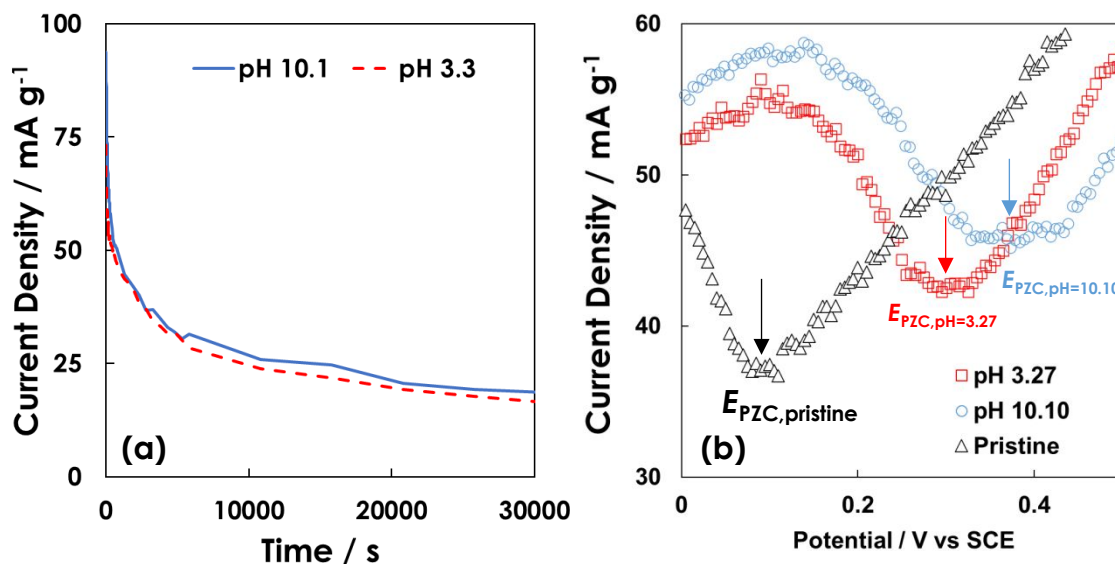


Figure 3. (a) Chronoamperometric treatment of the Kynol electrode at 0.8 V vs. SCE for 32,000 s in the NaCl solution with adjusted pH of 10.1 and 3.3, in which the total ionic strength is kept at 4.3 mM. (b) After chronoamperometry, voltammetry at 0.5 mV s⁻¹ was carried out to track the E_{PZC} for the treated electrode in 4.3 mM NaCl solution without pH adjustment. Voltammetry at 0.5 mV s⁻¹ for a pristine carbon cloth is also shown for comparison.

This experiment could be subsequently examined for a wide range of pH values with the rate of shift in E_{pzc} being dependent on the electrolyte pH and applied potential, among other factors such as electrolyte volume, purge conditions, and electrolyte composition as well as specific ion adsorption. For the purposes of this study, the carbon oxidation reaction is pH dependent is further confirmed through these stepped potentials, and it mirrors similar results in past works that has shown the degradation of a CDI system being dependent on the cell potential used to conduct the separation process.^{13, 31}

Carbon electrodes are used in both CDI and MCDI processes, but prior studies have shown the MCDI process is far more stable than a CDI process.³⁶ The main difference between these two systems lies in the ion-exchange membranes (IEMs). In MCDI, an anion exchange membrane is placed over the anode while a cation exchange membrane is placed over the cathode. These membranes are primarily meant to limit co-ion efficiency losses, meaning cations being desorbed at the anode and anions being desorbed from the cathode under an applied potential. These membranes may have an additional function such as stabilizing the local pH, therefore mitigating the pH-dependent carbon oxidation as discussed via Eq. (5-8). If carbon oxidation were to occur at the anode, the pH would be lowered due to the generation of protons as water reacts with the carbon surface, as shown in Eq. (5). These protons would be hindered from entering the bulk solution flow as they would need to first pass through an anion exchange membrane. While an anion exchange membrane cannot be expected to be 100% selective, it will likely hinder protons emanating from this reaction from entering the bulk solution. The creation of a locally acidic pH at the anode may decrease the oxidation rate of the carbon anode, mitigating Faradaic reaction and increasing the efficiency of the process. Likewise, at the cathode, if oxygen reduction were to occur, the hydroxide ions generated through that reaction would be hindered from meeting the bulk solution as they would need to pass through the cation exchange membrane first. In future studies, measurement of the concentration of ions at the carbon electrode-electrolyte interface in CDI and MCDI cells would also be useful.

To investigate the effect of IEMs on Faradaic reactions in CDI cells, the local pH conditions was examined in both CDI and MCDI systems. Cells were constructed with microporous carbon cloth electrodes at the anode and cathode, as shown in **Figure 2**. In the case of MCDI, a Neosepta anion

exchange membrane and a Neosepta cation exchange membrane were placed over the anode and cathode, respectively. The carbon electrodes were approximately 5 cm x 5 cm with IEMs completely covering the carbon surfaces. Near electrode pH probes were used to track the dynamic pH environment at the electrode surfaces, and pH and current were tracked as a function of stepped cell potentials. Charging and discharge were carried out for 30 min each.

Shown in **Figure 4a** and **4b** are the local pH response and current for the MCDI cell at a cell potential of 1.2 V after >70 hours of cycling. The local pH at the anode remains acidic under charging and discharging conditions, with the pH slightly decreasing under potential down to 2.9 and then slightly rising when the cell was short-circuited. The local pH at the cathode stays basic, approximately 11.3, under both charging and discharging conditions as well. The steady-state current at the end of the charging cycle is 3.8 mA. Shown in **Figure 4c** and **4d** are the local pH response and current for the CDI cell at a cell potential of 1.2 V. Unlike the MCDI cell, large fluctuations in the pH are seen under charging and discharging steps. The pH of both the anode and cathode return to close to neutral when discharging but diverge rapidly when under charging conditions. The pH at the anode reaches nearly 2.7 at the end of the charging cycle while the cathode reaches a pH of 10.3. The ability of the bulk solution to easily and quickly access the bulk of the carbon electrode results in these transient pH responses in the CDI cell while the IEMs in the MCDI cell limit this process. At the end of each discharging cycle, the anode in a CDI cell is returned to a more basic pH, increasing the magnitude of the overpotential towards carbon oxidation at the start of the next charging cycle. The steady-state current in the CDI cell is approximately 5.1 mA, notably over 30% higher than the current in the MCDI cell, with higher peak current and overall charge. It should also be noted that the potential at the anode in both

cell configurations has been shown to be high enough for oxygen evolution to occur.^{29, 33, 36} However, oxygen evolution on carbon electrodes is typically quite unfavorable kinetically, with heteroatom doping used to promote appreciable oxygen evolution rates.³⁷ Therefore, that reaction has generally been neglected here but is certainly worthy of mention. No visible gas evolution was seen in the outlet stream, but more work may be used to quantify any evolved gases.

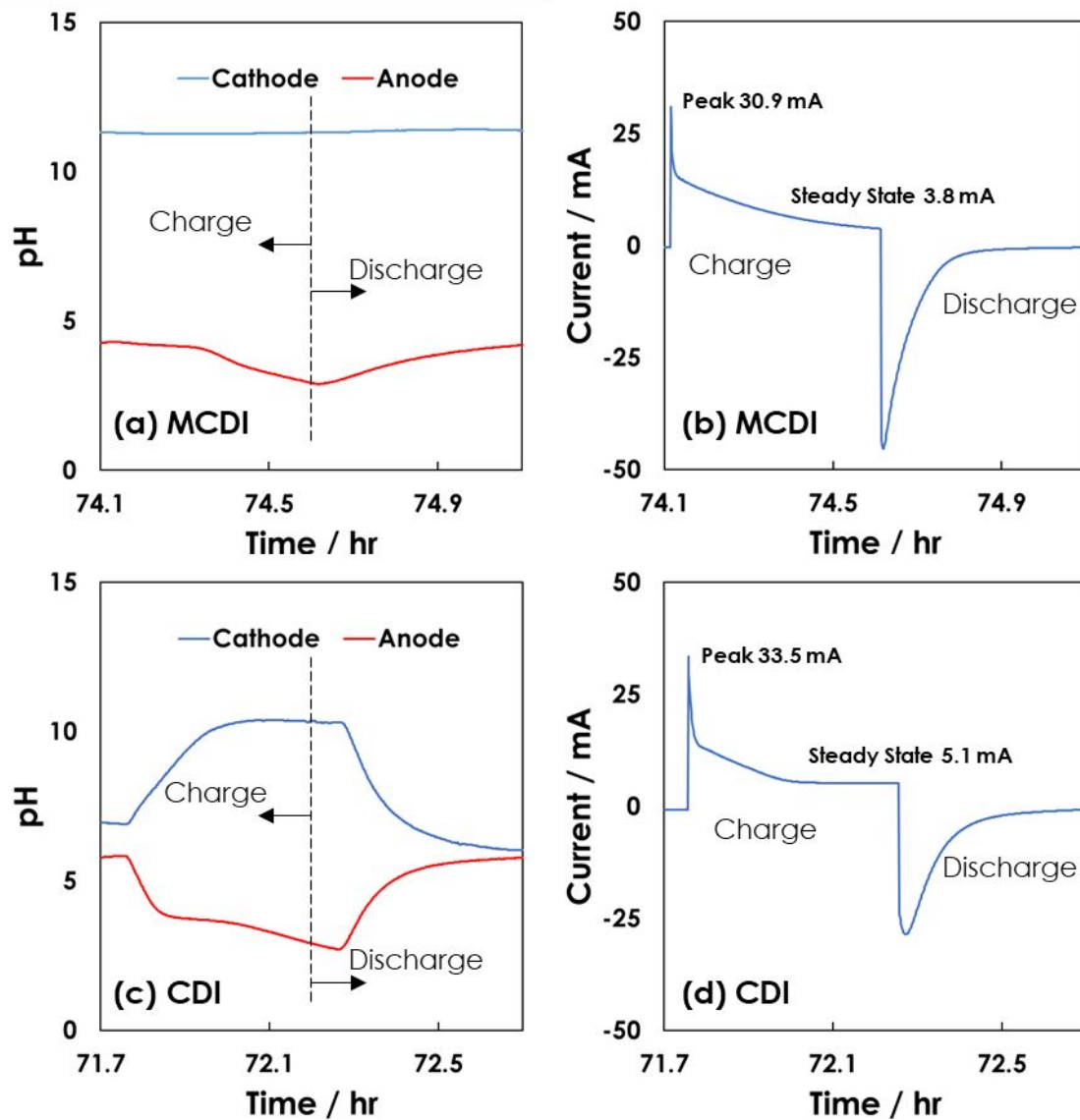


Figure 4. MCDI (a) pH and (b) current responses and CDI (a) pH and (b) current responses in a flow-by cell using an applied potential of 1.2 V in a 4.3 mM NaCl electrolyte with no nitrogen purging.

To investigate this effect further, the pH and current responses were examined for MCDI and CDI cells as a function of the cell potential. Cell potentials of 0.3, 0.6, 0.9, and 1.2 V were used for comparison, and the dynamic near electrode pH profiles are shown for both MCDI and CDI architectures are shown in **Figure S1** with **Figure S2** showing the outlet pH response after various time periods of cycling operation. As the potential is increased in both the MCDI and CDI cells, the pH at the anode and cathode diverges further. However, as was initially noted in **Figure 4**, the local pH does not return to near neutral in the MCDI cell and instead is relatively flat in between charging and discharging steps. In these experiments, the cell potential was progressively increased from 0.3 V through 1.2 V, leaving the local pH at the anode progressively more acidic and the pH at the cathode more basic. The steady-state current also rose in each cell as the cell potential was increased, although the magnitude of this increase in current was greater in the CDI cell than in the MCDI one. At cell potentials of 0.3, 0.6, 0.9, and 1.2 V, the steady-state currents in the MCDI cell were 0.4, 1.1, 1.9, and 3.8 mA, respectively. Likewise, in the CDI cell, at cell potentials of 0.3, 0.6, 0.9, and 1.2 V, the steady-state currents at the end of the charging cycle were 0.4, 1.4, 3.1, and 5.1 mA, respectively. These values highlight the protection against Faradaic current offered by the IEMs in the MCDI cell. However, these lower currents are also due to the reduced driving force for oxidation at the carbon anode due to the maintained locally acidic condition found at that electrode. These results mirror those found in the

chronoamperometry study mentioned earlier. It should also be noted that while similar conditions were maintained between experiments in this study, the inclusion of IEMs in the cell stack adds an extra resistive barrier that can aid in decreasing charging current, and also modulate pH and restrict dissolved oxygen access to the electrode to decrease parasitic faradaic current.³⁸ The anion exchange membrane (AEM) used here, AMX from Neosepta, has an ohmic resistance of $2.6 \Omega \cdot \text{cm}^2$ while the cation exchange membrane (CEM) used here, CMX from Neosepta, has an ohmic resistance of $1.8 \Omega \cdot \text{cm}^2$. With an overall area of 25 cm^2 for both the AEM and CEM and a peak current of 30.9 mA, the voltage drop from these IEMs is $<0.01 \text{ V}$. However, at higher current densities and further scale-up of these systems, the voltage drop from these IEMs cannot be neglected. The peak current seen in the MCDI cell was only 30.9 mA, while for the CDI cell, this value was also slightly higher at 33.5 mA.

While the steady-state current is lower in the MCDI cell, there still exists some current and therefore likely carbon oxidation taking place at the anode. Under similar conditions, carbon anodes in MCDI cells are expected to oxidize at a slower rate than in CDI cells. Pristine microporous carbon cloth as well as used cathodes and anodes from both the CDI and MCDI cells were examined using cyclic voltammetry (CV) to evaluate shifts in the E_{pzc} and subsequently degrees of oxidation to the carbon surface. Shown below in **Figure 5** are the resulting CVs for both of these cells. The cathode shows minor shifts in the E_{pzc} from -0.12 V vs. SCE to -0.03 V vs. SCE for the MCDI cell and to 0.01 V vs. SCE for the CDI cell. Oxidation of the carbon cathode may be due to reactions with hydrogen peroxide that is generated due to oxygen reduction. Larger shifts in the E_{pzc} were seen at the anode. The E_{pzc} shifted from -0.12 V vs. SCE to 0.09 V vs. SCE for the MCDI cell and to 0.28 V vs. SCE for the CDI cell. These results further confirm the protection

offered by the IEMs in the MCDI cell, which are not only important for limiting co-ion expulsion but also for creating local pH environments that will limit the extent of parasitic Faradaic reactions from occurring. The cation exchange membrane in the MCDI cell may also be responsible for limiting dissolved oxygen access to the cathode, something that has been shown in multiple previous works.^{4,27}

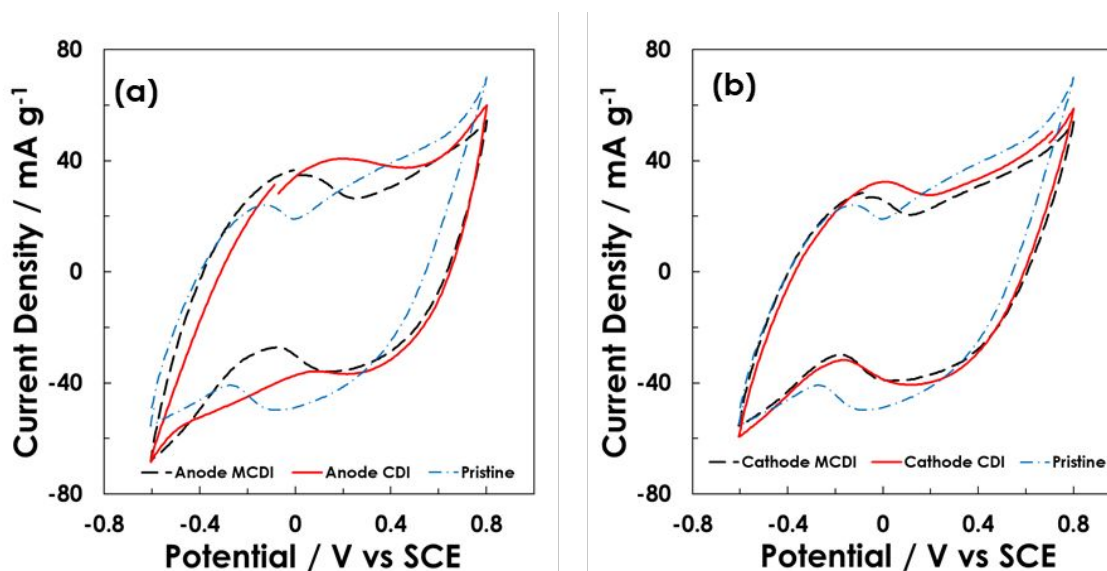


Figure 5. Changes in the cyclic voltammograms for the used (a) anode and (b) cathodes before and after the MCDI and CDI tests. The tests were performed at 0.5 mV s^{-1} in 4.3 mM NaCl solution.

Finally, the performance of the MCDI and CDI systems were assessed using conventional metrics of SAC and charge efficiency. Shown in **Figure 6** are the SAC and charge efficiency as a function of cell potential with values presented from an average of at least 3 cycles. Each system was run with a small solution volume of 400 ml that was recirculating at 20 ml/min , providing a turnover of 1.5 times during the 30 min charging process. These calculations are based on bulk changes in

the solution conductivity as registered by an in-line conductivity probe. The conductivity and current traces for MCDI and CDI cells at 0.3, 0.6, 0.9, and 1.2 V are shown in **Figure S3**. The SACs for the CDI studies ranged from approximately 0.9 to 5.5 mg/g while for the MCDI studies the range was notably higher with SACs from 1.5 to 15.5 mg/g. These SAC values are in line with most values seen for CDI systems, although the performance of the separation was not optimized for this process and was instead optimized for evaluating the near electrode pH values in a dynamic charging environment. The charge efficiencies were quite low for the CDI system, ranging from 38-50%. Charge efficiencies are conventionally lower for CDI systems due to co-ion expulsion phenomena and Faradaic reactions. The charge efficiencies for the MCDI system were significantly higher, between 62-99%, likely due to considerable mitigation of both co-ion expulsion and Faradaic reactions. No effort was made to purge the electrolyte of oxygen, which is one area of inefficiency that would have a higher impact in the CDI system. In addition, the electrode spacing between the anode and cathode was quite large, at 1.5 mm, which would add to decreases in the salt adsorption rate. Further evaluation of the pH and separation performance parameters is warranted in other test systems.

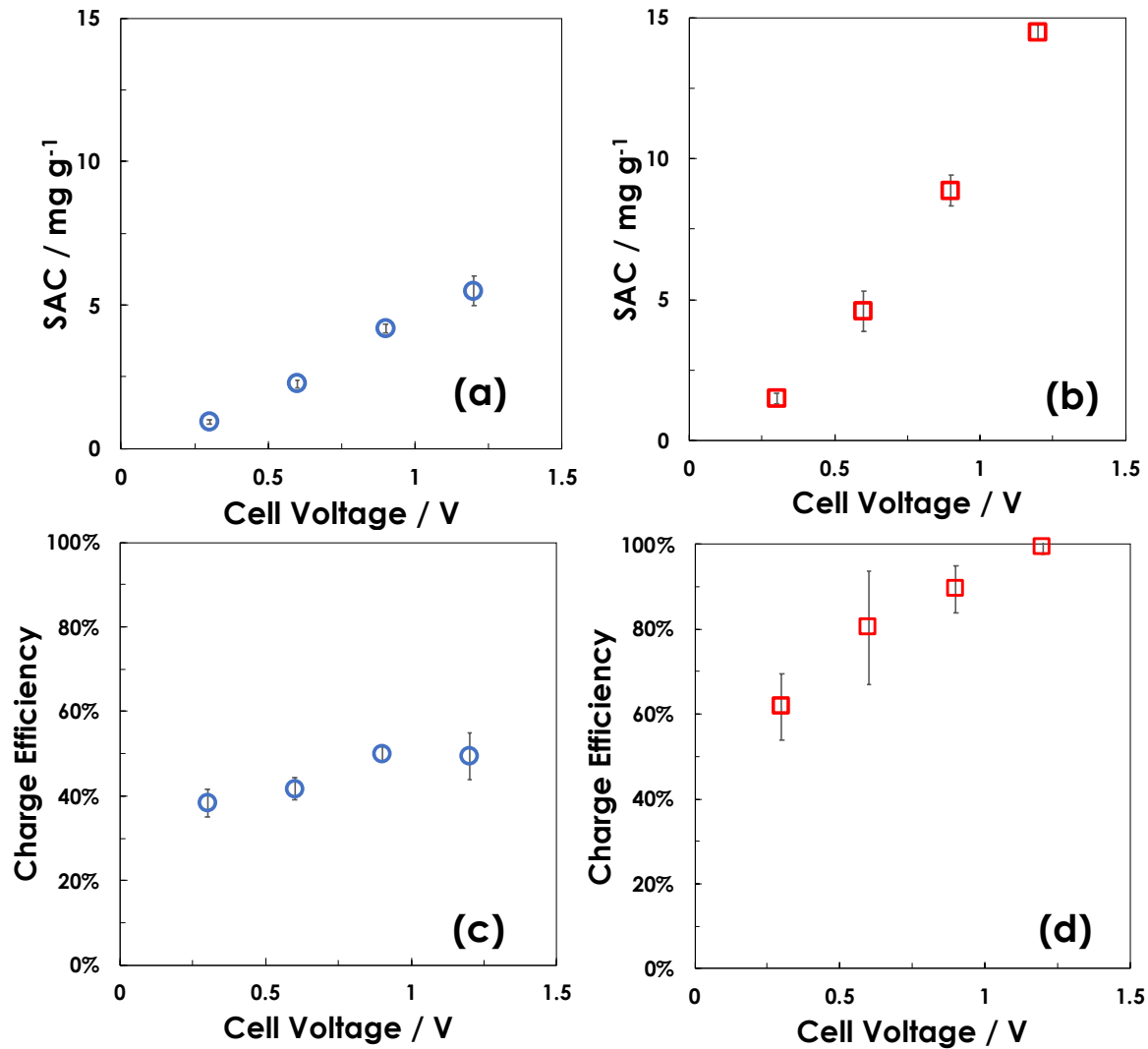


Figure 6. Salt adsorption capacity (SAC) for (a) CDI and (b) MCDI cells as a function of cell voltage. Charge efficiency for (c) CDI and (d) MCDI cells as a function of cell voltage.

The studies examined here were carried out with a flow-by cell using a single pair of electrodes. While flow-by cell results are expected to be analogous in other systems, they will not be exactly the same. For instance, the cell architecture will play a large role in the rate of carbon oxidation seen in a cell.³⁰ Cohen et al. showed that flow-by vs. flow-through will have a significant impact

on the rate of oxidation of the anode, which can also be attributed to local pH changes generated in the system. In a flow-through cell, the high pH generated at the carbon cathode will lead to a higher pH stream flowing into the anode, which is under an oxidizing potential. This higher pH will increase the overpotential and thereby driving force for the carbon oxidation reaction and subsequently increase the rate of oxidation seen in a flow-through cell versus a flow-by cell where typically the highest pH seen by the anode is the bulk solution pH. It should be further noted that in certain water streams the solution will be buffered, and in those systems, the pH swings at the anode and cathode will be more muted. More work is needed in more complex electrolytes to examine this point.

As a general outlook, cells will need to be designed that can maintain separation efficiencies with the local pH taken into account for the electrolyte chosen. In many recent papers, selective separations have been targeted by CDI cells.^{23, 39-41} However, the local conditions near the electrode surface will need to be examined in detail to determine the best conditions under which to operate the process. The inclusion of IEMs in these cells could further stabilize the separation and provide an additional design parameter when considering size-exclusion or other selective polymeric membranes.⁴² This research is an area of future development.

Conclusions

The local pH at an electrode surface has a direct impact on the overpotential for carbon oxidation and dissolved oxygen reduction in capacitive deionization cells. Electrochemical studies consisting of chronoamperometry and cyclic voltammetry were used to demonstrate that higher

solution pH will increase the extent of oxidation at a carbon electrode surface. Subsequently, local pH measurements and post-cycling examination of carbon electrodes in CDI and MCDI cells were analyzed. The transient local pH found in the CDI studies led to higher cell currents, lower separation performance, and more extensive oxidation of the carbon anode. In the MCDI study, lower currents combined with more stable pH conditions at the anode (acidic) and cathode (basic) lead to an overall reduction in Faradaic reactions and heightened separation performance. The use of ion exchange membranes provided multiple positive benefits towards enhancing the separation process. The results found here may be used to further benefit next generation CDI systems.

Conflict of interest

There are no conflicts of interest to declare.

Acknowledgements

The authors are grateful to the U.S.–China Clean Energy Research Center, U.S. Department of Energy for project funding (No. DE-PI0000017).

References

1. M. Qin, A. Deshmukh, R. Epsztein, S. K. Patel, O. M. Owoseni, W. S. Walker and M. Elimelech, Comparison of energy consumption in desalination by capacitive deionization and reverse osmosis, *Desalination*, 2019, **455**, 100-114.
2. J. Landon, X. Gao, A. Omosebi and K. Liu, Progress and outlook for capacitive deionization technology, *Current Opinion in Chemical Engineering*, 2019, **25**, 1-8.

3. S. K. Patel, C. L. Ritt, A. Deshmukh, Z. Wang, M. Qin, R. Epsztein and M. Elimelech, The relative insignificance of advanced materials in enhancing the energy efficiency of desalination technologies, *Energy & Environmental Science*, 2020, **13**, 1694-1710.
4. A. Omosibi, X. Gao, N. Holubowitch, Z. Li, J. Landon and K. Liu, Anion Exchange Membrane Capacitive Deionization Cells, *Journal of The Electrochemical Society*, 2017, **164**, E242-E247.
5. M. A. Anderson, A. L. Cudero and J. Palma, Capacitive deionization as an electrochemical means of saving energy and delivering clean water. Comparison to present desalination practices: Will it compete?, *Electrochimica Acta*, 2010, **55**, 3845-3856.
6. S. Porada, R. Zhao, A. van der Wal, V. Presser and P. M. Biesheuvel, Review on the science and technology of water desalination by capacitive deionization, *Progress in Materials Science*, 2013, **58**, 1388-1442.
7. P. Liu, T. Yan, L. Shi, H. S. Park, X. Chen, Z. Zhao and D. Zhang, Graphene-based materials for capacitive deionization, *Journal of Materials Chemistry A*, 2017, **5**, 13907-13943.
8. S. Porada, A. Shrivastava, P. Bukowska, P. M. Biesheuvel and K. C. Smith, Nickel Hexacyanoferrate Electrodes for Continuous Cation Intercalation Desalination of Brackish Water, *Electrochimica Acta*, 2017, **255**, 369-378.
9. X. Su, K.-J. Tan, J. Elbert, C. Rüttiger, M. Gallei, T. F. Jamison and T. A. Hatton, Asymmetric Faradaic systems for selective electrochemical separations, *Energy & Environmental Science*, 2017, **10**, 1272-1283.
10. C. Santos, J. J. Lado, E. García-Quismondo, I. V. Rodríguez, D. Hospital-Benito, J. Palma, M. A. Anderson and J. J. Vilatela, Interconnected metal oxide CNT fibre hybrid networks for current collector-free asymmetric capacitive deionization, *Journal of Materials Chemistry A*, 2018, **6**, 10898-10908.

11. S. Hand, X. Shang, J. S. Guest, K. C. Smith and R. D. Cusick, Global Sensitivity Analysis To Characterize Operational Limits and Prioritize Performance Goals of Capacitive Deionization Technologies, *Environmental Science & Technology*, 2019, **53**, 3748-3756.
12. X. Gao, A. Omosebi, J. Landon and K. Liu, Enhanced Salt Removal in an Inverted Capacitive Deionization Cell Using Amine Modified Microporous Carbon Cathodes, *Environmental Science & Technology*, 2015, **49**, 10920-10926.
13. X. Gao, A. Omosebi, J. Landon and K. Liu, Surface charge enhanced carbon electrodes for stable and efficient capacitive deionization using inverted adsorption–desorption behavior, *Energy & Environmental Science*, 2015, **8**, 897-909.
14. X. Gao, S. Porada, A. Omosebi, K. L. Liu, P. M. Biesheuvel and J. Landon, Complementary surface charge for enhanced capacitive deionization, *Water Research*, 2016, **92**, 275-282.
15. A. Omosebi, X. Gao, J. Landon and K. Liu, Asymmetric Electrode Configuration for Enhanced Membrane Capacitive Deionization, *ACS Applied Materials & Interfaces*, 2014, **6**, 12640-12649.
16. S. K. Patel, M. Qin, W. S. Walker and M. Elimelech, Energy Efficiency of Electro-Driven Brackish Water Desalination: Electrodialysis Significantly Outperforms Membrane Capacitive Deionization, *Environmental Science & Technology*, 2020, **54**, 3663-3677.
17. A. Omosebi, Z. Li, N. Holubowitch, X. Gao, J. Landon, A. Cramer and K. Liu, Energy recovery in capacitive deionization systems with inverted operation characteristics, *Environmental Science: Water Research & Technology*, 2020, **6**, 321-330.
18. D. Moreno and M. C. Hatzell, Constant chemical potential cycles for capacitive deionization, *Physical Chemistry Chemical Physics*, 2019, **21**, 24512-24517.
19. L. Wang, J. E. Dykstra and S. Lin, Energy Efficiency of Capacitive Deionization, *Environmental Science & Technology*, 2019, **53**, 3366-3378.

20. D. Moreno and M. C. Hatzell, Efficiency of Carnot and Conventional Capacitive Deionization Cycles, *The Journal of Physical Chemistry C*, 2018, **122**, 22480-22486.
21. P. Długolecki and A. van der Wal, Energy Recovery in Membrane Capacitive Deionization, *Environmental Science & Technology*, 2013, **47**, 4904-4910.
22. L. Wang and S. Lin, Intrinsic tradeoff between kinetic and energetic efficiencies in membrane capacitive deionization, *Water Research*, 2018, **129**, 394-401.
23. S. Hand and R. D. Cusick, Emerging investigator series: capacitive deionization for selective removal of nitrate and perchlorate: impacts of ion selectivity and operating constraints on treatment costs, *Environmental Science: Water Research & Technology*, 2020, **6**, 925-934.
24. L. Wang and S. Lin, Mechanism of Selective Ion Removal in Membrane Capacitive Deionization for Water Softening, *Environmental Science & Technology*, 2019, **53**, 5797-5804.
25. J. E. Dykstra, K. J. Keesman, P. M. Biesheuvel and A. van der Wal, Theory of pH changes in water desalination by capacitive deionization, *Water Research*, 2017, **119**, 178-186.
26. J. Yu, K. Jo, T. Kim, J. Lee and J. Yoon, Temporal and spatial distribution of pH in flow-mode capacitive deionization and membrane capacitive deionization, *Desalination*, 2018, **439**, 188-195.
27. W. Tang, D. He, C. Zhang, P. Kovalsky and T. D. Waite, Comparison of Faradaic reactions in capacitive deionization (CDI) and membrane capacitive deionization (MCDI) water treatment processes, *Water Research*, 2017, **120**, 229-237.
28. D. He, C. E. Wong, W. Tang, P. Kovalsky and T. D. Waite, Faradaic Reactions in Water Desalination by Batch-Mode Capacitive Deionization, *Environmental Science & Technology Letters*, 2016, **3**, 222-226.
29. X. Gao, A. Omojebi, Z. Ma, F. Zhu, J. Landon, M. Ghorbanian, N. Kern and K. Liu, Capacitive deionization using symmetric carbon electrode pairs, *Environmental Science: Water Research & Technology*, 2019, **5**, 660-671.

30. I. Cohen, E. Avraham, Y. Bouhadana, A. Soffer and D. Aurbach, The effect of the flow-regime, reversal of polarization, and oxygen on the long term stability in capacitive de-ionization processes, *Electrochimica Acta*, 2015, **153**, 106-114.
31. X. Gao, A. Omosebi, J. Landon and K. Liu, Dependence of the Capacitive Deionization Performance on Potential of Zero Charge Shifting of Carbon Xerogel Electrodes during Long-Term Operation, *Journal of The Electrochemical Society*, 2014, **161**, E159-E166.
32. J.-H. Choi, Determination of the electrode potential causing Faradaic reactions in membrane capacitive deionization, *Desalination*, 2014, **347**, 224-229.
33. B. Shapira, E. Avraham and D. Aurbach, Side Reactions in Capacitive Deionization (CDI) Processes: The Role of Oxygen Reduction, *Electrochimica Acta*, 2016, **220**, 285-295.
34. E. Avraham, M. Noked, A. Soffer and D. Aurbach, The feasibility of boron removal from water by capacitive deionization, *Electrochimica Acta*, 2011, **56**, 6312-6317.
35. N. Holubowitch, A. Omosebi, X. Gao, J. Landon and K. Liu, Quasi-Steady-State Polarization Reveals the Interplay of Capacitive and Faradaic Processes in Capacitive Deionization, *ChemElectroChem*, 2017, **4**, 2404-2413.
36. A. Omosebi, X. Gao, J. Rentschler, J. Landon and K. Liu, Continuous operation of membrane capacitive deionization cells assembled with dissimilar potential of zero charge electrode pairs, *Journal of Colloid and Interface Science*, 2015, **446**, 345-351.
37. L. Zhang, J. Xiao, H. Wang and M. Shao, Carbon-Based Electrocatalysts for Hydrogen and Oxygen Evolution Reactions, *ACS Catalysis*, 2017, **7**, 7855-7865.
38. J. E. Dykstra, R. Zhao, P. M. Biesheuvel and A. van der Wal, Resistance identification and rational process design in Capacitive Deionization, *Water Research*, 2016, **88**, 358-370.
39. W. Tang, D. He, C. Zhang and T. D. Waite, Optimization of sulfate removal from brackish water by membrane capacitive deionization (MCDI), *Water Research*, 2017, **121**, 302-310.

40. J. J. Lado, R. E. Pérez-Roa, J. J. Wouters, M. I. Tejedor-Tejedor, C. Federspill, J. M. Ortiz and M. A. Anderson, Removal of nitrate by asymmetric capacitive deionization, *Separation and Purification Technology*, 2017, **183**, 145-152.
41. S. A. Hawks, M. R. Cerón, D. I. Oyarzun, T. A. Pham, C. Zhan, C. K. Loeb, D. Mew, A. Deinhart, B. C. Wood, J. G. Santiago, M. Stadermann and P. G. Campbell, Using Ultramicroporous Carbon for the Selective Removal of Nitrate with Capacitive Deionization, *Environmental Science & Technology*, 2019, **53**, 10863-10870.
42. P. Nativ, O. Lahav and Y. Gendel, Separation of divalent and monovalent ions using flow-electrode capacitive deionization with nanofiltration membranes, *Desalination*, 2018, **425**, 123-129.